



Hydrophobicity enhancement of Ti-MWW catalyst and its improvement in oxidation activity



Hong Zhao^{a,b}, Toshiyuki Yokoi^{a,*}, Junko N. Kondo^a, Takashi Tatsumi^a

^a Chemical Resources Laboratory, Tokyo Institute of Technology, Nagatsuta 4259, Midori-ku, Yokohama 226-8503, Japan

^b Shanghai Advanced Research Institute, Chinese Academy of Sciences, 100 Haik Road, Zhangjiang Hi-Tech Park, Pudong, Shanghai 201210, PR China

ARTICLE INFO

Article history:

Received 14 April 2015

Received in revised form 25 June 2015

Accepted 3 July 2015

Available online 11 July 2015

Keywords:

Ti-MWW

Preparation conditions

Hydrophobicity

Catalytic activity

ABSTRACT

The effect of the preparation conditions of the Ti-MWW catalyst on the hydrophobicity of the catalyst and its catalytic activity was investigated. Our findings demonstrated that the condensation of interlayer hydroxyl groups was greatly affected by the preparation conditions, in particular washing conditions of the as-synthesized lamellar precursor of Ti-MWW, then further controlling the final hydrophobicity and oxidation properties. Using organic solvents, especially EAOH, instead of water to wash the wet lamellar precursor would synchronize the interlayer hydroxyl condensation with the decrease of interlayer distance mainly caused by the leaching of piperidine, which was used as structure-directing agent (SDA). After acid-treatment, less SDA was kept in the EAOH washed sample and 3D-MWW with less defects was formed by calcination. Both drying temperature and acid-treatment would also affect the amount of SDA occluded in the interlayer void space of the acid-treated samples and then further affect the final interlayer hydroxyl condensation upon the following calcination. The lower both drying temperature and acid-treatment temperature were favorable to unequal interlayer dehydroxylation to form MCM-56, while higher drying temperature such as 150 °C not only caused the anatase phase in the calcined samples but also occluded more SDA molecules in the acid-treated samples which greatly affect the further interlayer hydroxyl condensation upon the calcination. Ti-MWW-OH-100 containing smallest amount of silanols and less defect sites showed the best hydrophobicity and the highest catalytic activity in 1-hexene oxidation.

© 2015 Elsevier B.V. All rights reserved.

1. Introduction

Titanium silicate-1 molecular sieve (TS-1), an extremely efficient and environment benign redox catalyst, has been considered to be a milestone in zeolite catalysis in 80th last century due to its unique properties in oxidation of small organic molecules with dilute hydrogen peroxide solutions under mild conditions [1–6]. During the past decades great efforts have therefore been concentrated on the synthesis and application of a variety of titanium zeolites and Ti-containing mesoporous materials with different structures and pore dimensions including TS-2 [7], Ti-MWW [8,9], Ti-MOR [10], Ti-MCM-38 [11], Ti-Beta [12–14], Ti-MCM-41/48 [15–20], Ti-SBA-15 [21–23] and Ti-containing polyhedral oligomeric silsesquioxanes (POSS) [24,25] and so on.

Although it is still a challenge to thoroughly understand why different Ti-catalysts seem to have different catalytic properties,

there is no doubt that the outstanding hydrophobicity of TS-1 plays a greatly important role in its unique behavior [26–28]. It is reported that TS-1 synthesized by microwave heating exhibited the higher selectivity in the epoxidation of styrene as well as the higher catalytic activity in the epoxidation reactions of 1-hexene and styrene than that synthesized by conventional heating [29]. The superiority of the former is considered to be directly caused by the enhanced surface hydrophobicity. Similar to TS-1, Camblor et al. [30] reported that aluminum-free Ti-Beta zeolite synthesized in fluoride had less Si-OH connectivity defects as opposed to that synthesized in OH⁻ media. This enhanced hydrophobicity of Ti-Beta (F) determines its higher activity and selectivity in the oxidation of organic substrates containing a polar moiety. Except from Ti-containing zeolites, Tatsumi report that silylated Ti-MCM-41 and Ti-MCM-48 exhibited enhanced catalytic activity in the epoxidation of olefins, as a result of increase in hydrophobicity [31]. Since then, several activity-improved Ti-containing mesoporous materials and even FAU zeolite supported TiO₂ photocatalyst [32] are reported by hydrophobicity enhancement through the direct or secondary incorporation of organic group [21,33].

* Corresponding author.

E-mail address: yokoi.t.ab@m.titech.ac.jp (T. Yokoi).

Ti-MWW, which possesses a unique pore structure comprised of two independent 10-membered-ring (MR) channels and 12-MR cups on the crystal exterior, has proved to be much more active than TS-1 and Ti-Beta in the epoxidation of linear alkenes with H_2O_2 [8] and it was used in various organic reactions [34–37]. However, MWW lamellar precursor is very flexible and condition-sensitive. Through different post treatments it is readily converted into MCM-22, MCM-36 [38], MCM-56 [39], ITQ-2 [40] and IEZ-MWW [41]. It is also these futures of MWW precursor that makes MWW sheets very difficult to stack together regularly and orderly and to form more rigid and perfect 3D MWW structure with T-O-T linkages upon the calcination. Ti-MWW with more hydroxyl groups was caused by the incomplete interlayer dehydroxylation. This means that there is much space for us to improve the Ti-MWW catalytic properties by hydrophobicity enhancement.

Through the incorporation of organic groups into the porous materials can effectively improve the property of Ti-containing mesoporous catalysts, but this method is not necessarily the most suitable one for Ti-MWW due to the relatively smaller pore channel. Wang et al. report that the post treatment of 3D Ti-MWW with PI/HMI can induce the reversible structural rearrangement of firstly deboronated Ti-MWW and efficiently improve the hydrophobicity and oxidation activity of Ti-MWW [42]. Nevertheless, this post hydrothermal treatment with PI/HMI not only increases the cost but also complicates the preparation process.

Up to now, Ti-MWW is necessarily prepared from the very flexible and condition-sensitive lamellar precursor through washing, drying, acid-treatment and the following calcination. Inevitably, the preparation conditions, which affect the condensation of hydroxyl groups, control the final hydrophobicity followed by the oxidation properties of Ti-MWW. This means that it is entirely possible for us to control the hydrophobic/hydrophilic properties of Ti-MWW by controlling the preparation conditions. This assumption is well applied by our current work.

Here we show a very convenient and efficient way to enhance the hydrophobicity and improve the property of Ti-MWW. Use of EAOH instead of pure water to wash wet crystals after crystallization was the key to prepare highly hydrophobic Ti-MWW catalysts. The following drying and acid-treatment also have great effect on the Ti-MWW hydrophobicity. Choosing 1-hexene epoxidation as the probe reaction, a detailed study describing the effect of preparation conditions on the physiochemical properties and catalytic behavior of Ti-MWW materials is presented.

2. Experimental

2.1. Catalyst preparation and characterization

The layered precursor of the MWW titanosilicate, Ti-MWW (P), was hydrothermally synthesized using piperidine (PI) as structure-directing agent (SDA) and boric acid as crystallization-supporting agent according to the literature with our slight modifications [8]. The gels with the molar compositions of 1.0 SiO_2 :0.033 TiO_2 :1.4 PI:0.67 B_2O_3 :19 H_2O were crystallized under rotation (20 rpm) at 170 °C for 7.5 days. After the hydrothermal treatment, the wet crystals were washed by three times volume of water or EAOH three times and then dried at 30–150 °C for 24 h. This sample was denoted as Ti-MWW (P)-X-Y, where X and Y were the washing solution and the drying temperature, respectively. For example, when the washing solvent was EAOH and the drying temperature was 100 °C, the sample was designated as Ti-MWW-EAOH-100. Ti-MWW (P)-X-Y was acid-treated at 100 °C for 20 h and further calcined at 550 °C for 10 h to obtain Ti-MWW-X-Y, which has 3D MWW structure. The series of the Ti-MWW catalysts were prepared from the same batch of the Ti-MWW lamellar precursor (Ti-MWW (P)). Table 1

summarized the compositions and physical properties of the prepared catalysts under the different conditions.

The X-ray diffraction (XRD) patterns were recorded on a MAC Science M₃X 1030 X-ray diffractometer with Cu source ($\lambda\alpha_1 = 1.54056 \text{ \AA}$, $\lambda\alpha_2 = 1.54439 \text{ \AA}$, 40 kV, 20 mA) to identify the crystalline phase and calculate unit-cell parameters. The titanium coordination states of the as-synthesized and calcined materials were investigated by diffuse reflectance (DR) UV-vis spectroscopy (JASCO V-550 UV-vis spectrophotometer). OH-region infrared (IR) spectra were measured on a PE-1600 FTIR spectrometer. Before recording the spectra in the OH stretching vibration region, the samples were first evacuated at 500 °C for 2.5 h under high-vacuum conditions and then cooled to room temperature. ²⁹Si MAS NMR measurements were performed on a JEOL ECA-400 nuclear magnetic resonance spectrometer at ambient temperature. N_2 adsorption at –196 °C and H_2O adsorption at 25 °C were carried out on Belsorp 28SCA and Belsorp 18SCA instruments, respectively. TG/DTA was measured on an ULVAC-Rigaku TGD 9600 thermal analysis system. The temperature was ramped to 800 °C at a heating rate of 10 °C min^{–1}. The amounts of Ti and B of the samples were determined by inductively coupled plasma-atomic emission spectrometry (Shimadzu ICPS-8000E). Scanning electron microscopy (SEM) was performed on a JEOL JSMT220 instrument.

2.2. Catalytic reactions

The epoxidation of 1-hexene with H_2O_2 , which was used as the probe reaction, was performed by batchwise in a 25-mL flask equipped with a magnetic stirrer and a condenser. Typically, the mixture containing 50 mg Ti-MWW catalyst, 10 mL of MeCN, 10 mmol of 1-hexene and 10 mmol of H_2O_2 was stirred vigorously at 60 °C for 2 h. After the catalyst was removed, the products were analyzed on a gas chromatograph (Shimadzu 14B, FID detector) equipped with a 50 m DB-1 capillary column. The amount of unconverted H_2O_2 was quantified by standard titration method with 0.1 M $Ce(SO_4)_2$ solution.

3. Results

3.1. Ti-MWW synthesis and characterization

3.1.1. Washing solution

The influence of washing solution on the structure was investigated using the samples dried at 100 °C as representatives. Fig. 1 showed the XRD patterns of the precursors washed by water or EAOH and the correspondingly calcined samples. Ti-MWW (P)-EAOH-100 showed the same XRD patterns as Ti-MWW (P)- H_2O -100 and the both calcined samples exhibited the typical MWW structure, indicating that washing solution had no significant influence on the structure and crystallinity of both the precursor and the corresponding calcined Ti-MWW samples. Scanning electron micrographs (SEM) (not shown here) and N_2 adsorption results (shown in Table 1) revealed that the washing solution had little effect on the hexagonal morphology and crystal size distribution or surface area and pore volume of the calcined samples.

3.1.2. Drying temperature

In order to investigate the influence of the drying temperature on the structure of Ti-MWW, the samples washed with EAOH dried at 30, 70, 100 and 150 °C were used as representatives. The XRD patterns of precursors were showed in Fig. 1. Clearly, the patterns of Ti-MWW(P)-EAOH-30, Ti-MWW(P)-EAOH-70 and Ti-MWW(P)-EAOH-100 were totally consistent with that of the typical lamellar precursor of the MWW topology. However the pattern of Ti-MWW(P)-EAOH-150 was a very close approximation assigned

Table 1

Preparation conditions and physicochemical properties of Ti-MWW catalysts.*

Sample	Structure	Si/Ti ^a	Si/B ^a	S_{BET} (m^2/g) ^b	S_{ext} (m^2/g) ^b	V_{micro} ^b
Ti-MWW-EAOH-30	MCM-56	57	44	451	151	0.13
Ti-MWW-EAOH-70	MWW	63	36	546	142	0.16
Ti-MWW-H ₂ O-100	MWW	59	35	532	138	0.17
Ti-MWW-EAOH-100	MWW	62	41	536	137	0.16
Ti-MWW-EAOH-150	MWW	65	39	520	124	0.17

* All samples were prepared from the same batch of wet lamellar crystals.

^a Given by ICP.

^b Given by N₂ adsorption for calcined samples.

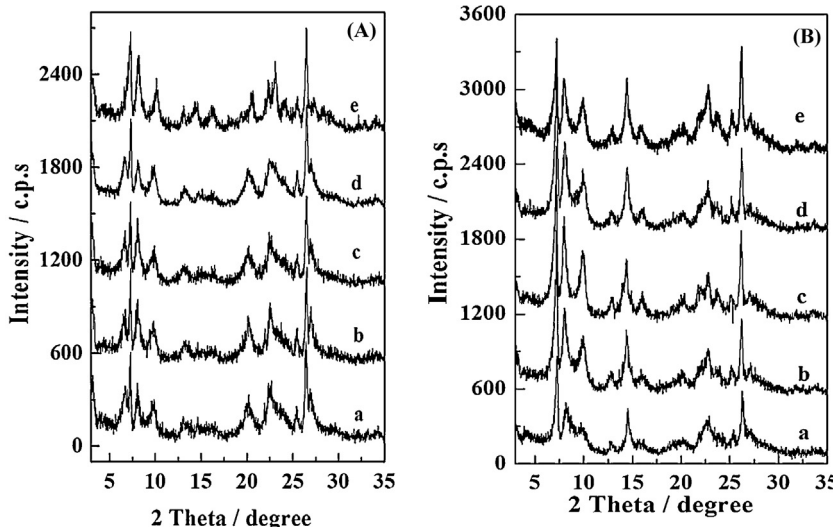


Fig. 1. (A) XRD patterns of (a) Ti-MWW(P)-EAOH-30, (b) Ti-MWW(P)-EAOH-70 °C, (c) Ti-MWW(P)-EAOH-100 °C, (d) Ti-MWW(P)-H₂O-100 and (e) Ti-MWW(P)-EAOH-150 °C; (B) XRD patterns of (a) Ti-MWW-EAOH-30, (b) Ti-MWW-EAOH-70, (c) Ti-MWW-EAOH-100, (d) Ti-MWW-H₂O-100 and (e) Ti-MWW-EAOH-150.

to the (001) and (002) diffraction lines of lamellar MWW precursor nearly disappeared, while the peaks due to the indexes of h00 and hk0 remained practically unchanged, indicating the structural change evolved along the c-axis and the loss of the lamellar structure.

Upon acid-treatment and further calcination, the XRD pattern of Ti-MWW-EAOH-70, Ti-MWW-EAOH-100 and Ti-MWW-EAOH-150 were shown in Fig. 1(B), indicating the characteristic diffractions due to the 100, 101, and 102 planes of the MWW structure but with the absence of the 001 and 002 peaks due to the layered structure, which was fully consistent with that of the well-known 3D MWW structure. However, the XRD patterns of Ti-MWW-EAOH-30 (trace a) showed that there was a marked difference in the 101 and 102 diffractions associated with the c-axis. Clearly, the intensity of the 101 peak decreased and the 102 peak broadened seriously. It was well established that the broadband in the region of 7.5–11° can be taken as evidence for the formation of a structure analog to MCM-56 which was a disordered collection of the MWW sheets apparently along c direction [39]. It suggested that the MWW sheets of Ti-MWW-EAOH-30 were at least not an ordered arrangement as that of typical 3D-MWW structure. Moreover, the sample prepared by washing and followed direct acid-treatment and calcination but not drying showed a typical XRD pattern of MCM-56 (not shown). The XRD results of these samples matched well with the textual characteristics obtained from N₂ adsorption isotherm shown in Table 1. These results implied that the drying process before acid-treatment was essential to prepare the 3D MWW structural sample and that lower drying temperature such as 30 °C, similar to the reported lower acid-treatment temperature [43], resulted in a disordered collection of MWW sheets apparently along c direction to form MCM-56.

Fig. 2(A) and (B) showed the UV spectra of the Ti-MWW catalysts prepared at different conditions. It can be seen that Ti-MWW (P)-EAOH-100 and Ti-MWW (P)-H₂O-100 exhibited a main band at 260 nm together with a weak shoulder around 220 nm, which were attributed to the octahedral and/or dimeric Ti derivatives and the tetrahedrally coordinated Ti species highly dispersed in the framework, respectively. After the acid-treatment at 100 °C for 20 h, the band at about 260 nm disappeared and both Ti-MWW-EAOH-100 and Ti-MWW-H₂O-100 showed only a narrow band at 220 nm. This result implied that the washing solution had no obvious effect on the Ti species coordination in the precursors or the acid-treated and further calcinated samples. However, it should be noted that the precursor dried at 150 °C showed another obvious band at about 330 nm which was assigned to an anatase-like Ti phase. After the acid-treatment and further calcination, the band at about 260 nm disappeared but the obvious band at around 330 nm was still kept. These findings indicated that the anatase formed in the precursor dried at higher temperature could withstand the acid extraction and was hardly removed and that high drying temperature was harm to prepare the anatase-free samples.

3.2. Hydrophobicity of the prepared Ti-MWW

The IR spectra in the region of the hydroxyl stretching vibration, ²⁹Si MAS NMR and water adsorption measurements were employed to correlate the preparation conditions and hydrophobicity using Ti-MWW-EAOH-30, Ti-MWW-EAOH-100, Ti-MWW-EAOH-150 and Ti-MWW-H₂O-100 as representatives. Fig. 2(C) showed the IR spectra in the region of hydroxyl stretching and Table 2 showed the band area integrated in the range of 3000–3900 cm⁻¹. The band at 3745 cm⁻¹ was assigned to the

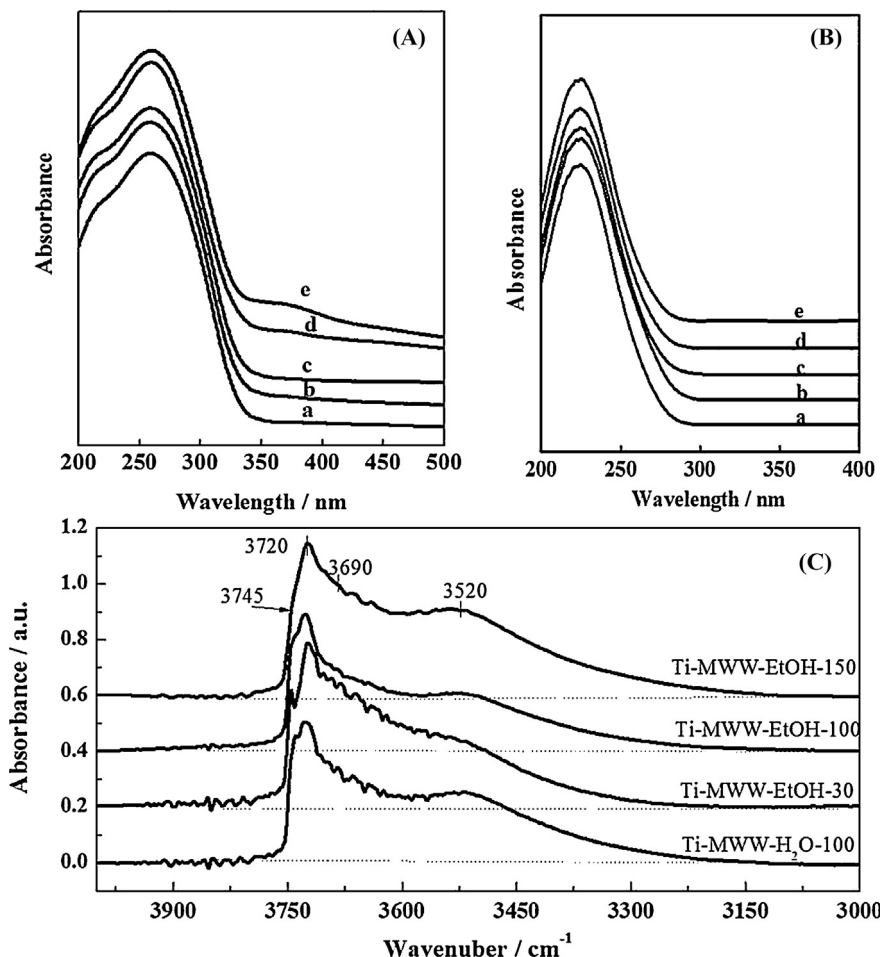


Fig. 2. UV-visible spectra of (A) as-synthesized and (B) calcined Ti-MWW-H₂O-100 (a) and Ti-MWW-EAOH-X. X = 30 (b), 70 (c), 100 (d) and 150 (e); (C) IR spectra in region of hydroxyl stretching vibration of Ti-MWW samples.

Table 2
Hydrophobicity of Ti-MWW catalysts.

Sample	$S_{IR(3850-3100\text{cm}^{-1})}$ ^a	$V[\text{cm}^{-3}(\text{STP})\text{g}^{-1}]$ ^b
Ti-MWW-EAOH-30	131	101
Ti-MWW-EAOH-100	82	79
Ti-MWW-H ₂ O-100	117	95
Ti-MWW-EAOH-150	159	114

^a $S_{IR(3850-3100\text{cm}^{-1})}$: determined from the OH stretching in IR spectra (3900–3000 cm⁻¹).

^b $V[\text{cm}^{-3}(\text{STP})\text{g}^{-1}]$: given by H₂O adsorption isotherms at 25 °C.

isolated external or terminal silanols on the crystal surface. The band at 3720 cm⁻¹ probably due to asymmetric hydrogen-bonded silanols located inside the crystals, the band at 3690 cm⁻¹ assigned to vicinal silanols and the broad band at around 3520 cm⁻¹ due to hydrogen-bonded silanols nests were also observed. Compared with Ti-MWW-H₂O-100, Ti-MWW-EAOH-100 showed much weaker bands at 3745 cm⁻¹, 3690 cm⁻¹ and 3520 cm⁻¹. The latter two bands were due to the internal silanols of Ti-MWW which originate from the defect sites as a result of deboronation and/or incomplete interlayer dehydroxylation [42]. Note that the boron amount in Ti-MWW-H₂O-100 was a little higher than that in Ti-MWW-EAOH-100 (Table 1). This implied that a large number of internal silanols in the Ti-MWW-H₂O-100 were mainly caused by the incomplete interlayer dehydroxylation.

Drying temperature also showed great influence on the OH stretching vibrations. Ti-MWW-EAOH-150 showed the greatest band area integrated in the range of 3000–3900 cm⁻¹, suggesting

that it had the most silanols in the framework. Ti-MWW-EAOH-30 gave a very intensive band at 3745 cm⁻¹, which should be firmly related to an open structure of MCM-56. This was in good agreement with the XRD patterns in Fig. 1(B) (trace a). Both MCM-56 prepared from lower drying precursor and that prepared at lower acid-treatment temperature were presumed to be a disordered collection of the MWW sheets along the c-axis. Hence, we can conclude that lower drying and lower acid-treatment temperatures made for the incomplete and unequal interlayer dehydroxylation.

To further probe the hydrophobicity of Ti-MWW catalysts, ²⁹Si MAS NMR spectroscopy was performed and showed in Fig. 3. The Q⁴ sites, where Qⁿ is Si(OM)_n(OH)_{4-n}, M = Si or Ti, in the region of -105 to -130 ppm were deconvoluted into five lines, which can be assigned to several distinctive crystallographic T sites in the MWW framework but with overlapping resonances [38,39]. In addition, an obvious resonance at -98 ppm attributed to the Q³ site, Si(OH)(OSi)₃ or Si(OH)(OTi)(OSi)₂. Ti-MWW-EAOH-100 showed very similar resonances due to the Q⁴ sites but a less intensive -98 ppm resonance due to the Q³ site compared to Ti-MWW-H₂O-100. This agreed well with the above IR spectra to verify the less defect sites in Ti-MWW-EAOH-100. Moreover, the spectra of Ti-MWW-EAOH-150 and Ti-MWW-EAOH-30 showed another well-resolved resonance in the downfield Q² site (-93 ppm), which was absent in the spectra of Ti-MWW-H₂O-100 and Ti-MWW-EAOH-100, being in good agreement with the above IR spectra that the strong band at 3520 cm⁻¹ was observed for both samples.

The amount of water adsorbed on samples was listed in Table 2 based on the water adsorption isotherms measurements. The

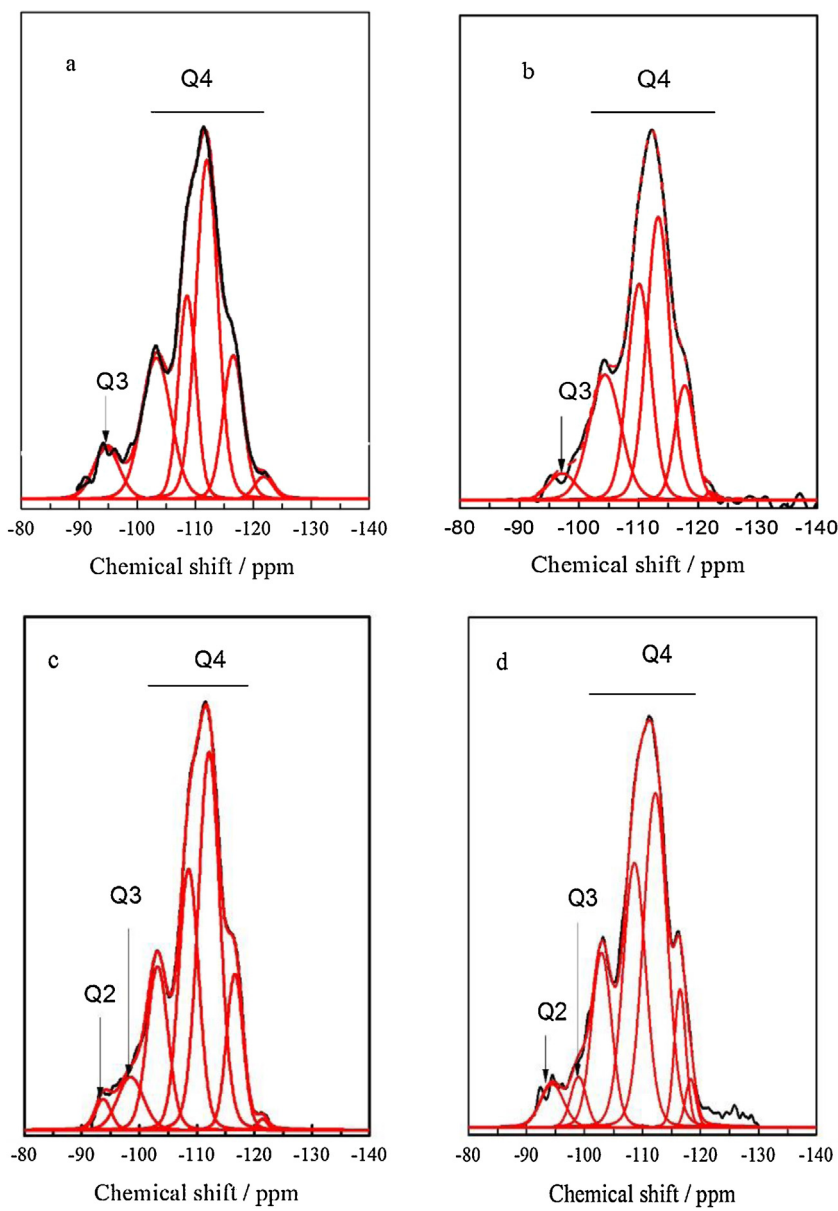


Fig. 3. ^{29}Si MAS NMR spectra of (a) Ti-MWW-H₂O-100, (b) Ti-MWW-EAOH-100, (c) Ti-MWW-EAOH-30 and (d) Ti-MWW-EAOH-150.

amount of the absorbed water on the Ti-MWW-EAOH-100 was the lowest compared with other four samples. This demonstrated that Ti-MWW-EAOH-100 was the most hydrophobic than other samples.

3.3. Catalytic properties of the prepared Ti-MWW

The oxidation of 1-hexene with H₂O₂ was used as the probe reaction to explore the Ti-MWW catalytic properties. The reaction was considered to be able to take place on all Ti species in Ti-MWW because of the relatively small molecular sizes of both the substrate and the oxidant without significant diffusion problems in the Ti-MWW structure [8,42]. Fig. 4(A) compared the turnover numbers (TON) of the Ti-MWW-EAOH and Ti-MWW-H₂O samples. In order to eliminate the effect of Ti content on TON, the Si/Ti ratio of the calcined samples was controlled at 60–65. Clearly, the EAOH-washed samples showed a higher TON than the H₂O-washed ones prepared under the same other preparation conditions; the TONs

of the EAOH-washed samples were almost twice as high as the H₂O-washed ones.

As a control, besides EAOH, other solutions such as acetonitrile and alcohols with different carbon atoms were also investigated to be used as washing solution. The Ti-MWW sample prepared by reversible structural rearrangement also used for comparison. The reaction results are summarized in Table 3, suggesting that the use of the organic solutions, except C₄-C₆OH which cannot wet the crystal precursor, in substitution for water can also improve the catalytic activities of the samples. Because EAOH was the most efficient, cheapest and environment-friendly, it was used as representative and was investigated detailedly. As verified by the IR spectra in the region of the hydroxyl stretching vibration, ^{29}Si MAS NMR and water adsorption measurements, the superior catalytic activity of the EAOH-washed samples was mainly caused by the enhanced hydrophobicity.

Fig. 4(A) also depicted the influence of the drying temperature on the catalytic activity of Ti-MWW. The TON for the 1-hexene oxidation showed a volcanic behavior over both Ti-MWW-OH and

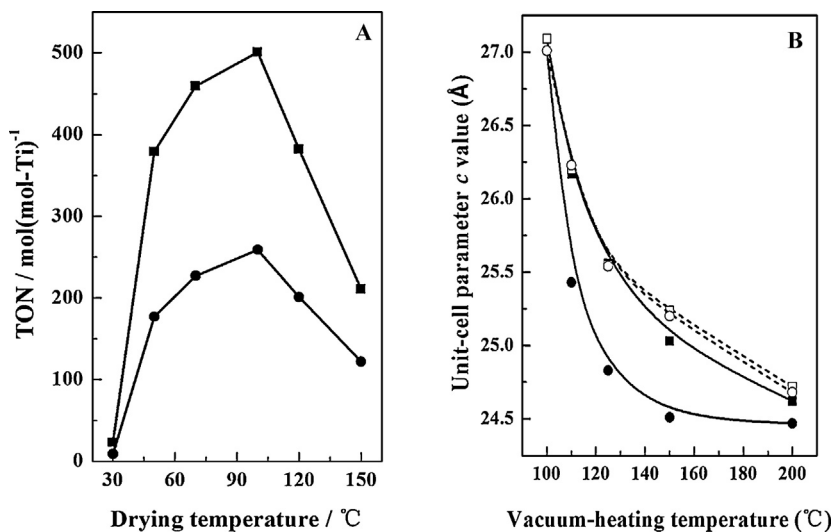


Fig. 4. (A) The comparison of TON between Ti-MWW-EAOH-Y (-●-) and Ti-MWW-H₂O-Y (-■-) ($Y = 30, 50, 70, 100, 120$ and 150); (B) unit-cell parameter c values of the outgassed Ti-MWW(P)-EAOH (-●-), Ti-MWW(P)-H₂O (-■-), the air-exposed Ti-MWW(P)-EAOH after outgas (-○-) and the air-exposed Ti-MWW(P)-H₂O after outgas (-□-).

Ti-MWW-H₂O. As described above, the samples prepared from the precursors dried at 30 °C were Ti-MCM-56 analogs and the activities of 1-hexene oxidation were very low. When the drying temperature was as high as 50 °C, the Ti-MWW samples after the acid-treatment followed by the calcination the TON values were increased greatly. The TON value over the both series was increased with an increase in the drying temperature and simultaneously reached the maximum values at about 100 °C. Further increasing the drying temperature, the hydrophobicity of the samples was decreased and the TON also decreased. Especially when the drying temperature was as high as 150 °C, anatase phase appeared and the activities of samples fell down sharply.

4. Discussion

In order to investigate the influence of organic washing solution on the transformation of the layered solid into Ti-MWW, we prepared a series of comparable samples from Ti-MWW(P)-EAOH-100 and Ti-MWW(P)-H₂O-100 by vacuumed at different temperatures for 16 h. The organic leaching upon vacuum-heating was detected by TG analysis and the unit-cell parameters were checked by XRD analysis. The XRD data were analyzed via Rietveld's refinement method [44] using the JADE 6.0 software. The background was fit manually and the line profiles were fit using pseudo-Voigt functions. P6/mmm structure, determined by Leonowicz et al. for

calcined MCM-22 [45], was used during the refinement process from 101 and 102 diffraction lines which were very intense and easy to accurately determine their positions and d -spacing values. Table 4 summarized the unit-cell parameters of these samples, and Fig. 4(B) showed the effect of vacuum-heating temperatures on the unit-cell parameter c . In order to clearly illustrate the change in the c values with the vacuum temperature, the start points in Fig. 4(B) were the values of the precursors but not the data got from the samples vacuumed at 100 °C. All samples showed similar unit-cell parameter a and b but different c values. Clearly, c values of both EAOH-washed samples and H₂O-washed samples were decreased with an increase in the vacuum-heating temperature, but the latter changed more sharply and acutely than the former. In detail, c value of EAOH-washed sample was decreased gradually along with the vacuum-heating temperature, and when the vacuum-heating temperature reached 200 °C, c value decreased to 24.62 Å and was much closed to that of calcined 3D-strutural sample. However, as for H₂O-washed samples, the c value was decreased sharply to 24.83 Å when the outgas temperature was 125 °C, and further raising vacuum temperature the c value changed little. Since the crystalline structure within layers is rigid, it suggested that the interlayer spacing of both the H₂O-washed and EAOH-washed samples was decreased with an increase in the vacuum temperature, and that the former changed more rapidly and acutely than the latter.

Table 3
Oxidation of 1-hexene^a with H₂O₂ over Ti-MWW^a

Sample	Conversion (%)	Selectivity (%)	H ₂ O ₂	
			Conversion (%)	Efficiency (%) ^b
Ti-MWW-CH ₃ OH	53.6	99.2	65.6	81.7
Ti-MWW-C ₂ H ₅ OH	55.6	99.5	62.5	89.0
Ti-MWW-C ₃ H ₇ OH	49.6	99.4	59.5	83.4
Ti-MWW-C(CH ₃) ₃ OH	31.3	98.9	35.3	88.7
Ti-MWW-C ₈ H ₁₇ OH	26.2	99.1	39.7	66.0
Ti-MWW-CH ₃ CH ₂ CHO	50.7	99.1	58.8	86.2
Ti-MWW-CH ₃ CN	51.9	99.4	58.1	89.3
Ti-MWW-H ₂ O	36.3	99.4	44.3	81.9
^c Re-Ti-MWW	58.7	99.3	69.3	84.7

^a Reaction conditions: catalyst (0.05 g), cyclohexene (10 mmol), H₂O₂ (10 mmol), acetonitrile (10 mL), temperature (60 °C), reaction time (2 h). The by-product was mainly diol checked by GC-MAS.

^b Ti-MWW samples were prepared from the same batch of lamellar crystals and Si/Ti in gel was 40. Drying temperature was 100 °C, acid-treatment temperature was 100 °C.

^c Re-Ti-MWW prepared according to [36], Si/Ti is 66.

Table 4

Refined unit-cell parameters of the vacuum-heated samples.

Vacuum temperature (°C)	EAOH washed sample		H ₂ O washed sample	
	a = b (Å)	c (Å)	a = b (Å)	c (Å)
— ^a	13.90	27.09	13.88	27.01
110	13.95	26.17	14.09	25.43
125	14.11	25.56	14.03	24.83
150	14.08	25.03	13.99	24.51
200	14.10	24.62	14.17	24.47

^a Precursors dried at 100 °C.

Table 5 showed the TG results of the above vacuumed samples. The weight losses, in the range of 200–700 °C derived from the total removal of PI molecules as SDA and in the range of 200–400 °C derived from the removal of PI molecules located at the void space between layers, were decreased with an increase in the vacuum-heating temperatures. However the much less weight loss occurred in the above two ranges of the H₂O-washed samples than in that of EAOH-washed samples. This implied that the more organic molecules were removed from the interlayer space and other place of water-washed samples than EAOH-washed samples at the same vacuum-heating temperature.

However, it was really important to note in Fig. 4(B) that c values were dramatically changes when the above outgassed samples were re-exposed to air atmosphere for 3 days at r.t. After exposure to air, the c values of water-washed samples were increased reversibly except that of the sample vacuum-heated at 200 °C, while the c values of almost all EAOH-washed samples were unchanged except for the one vacuumed at 150 °C, of which c value was increased from 25.03 to 25.24 Å. The difference between c values of H₂O-washed samples and EAOH-washed samples became very obscure and were only a function of vacuum-heating temperatures no matter with what washing solution were used or what the c values were before exposure to air atmosphere. Apparently, the interlayer spacing decrease upon vacuum-heating was mainly caused by the progressive elimination of organic molecules located between the layers. However, if there was no force to maintain the shrink of the interlayer space caused by organic molecules leaching, it was certainly easy to re-expand once the air and water molecules enter the interlayer space again.

From Fig. 4(B), the c values of both H₂O and EAOH washed samples outgassed at 200 °C were little changed after exposure to air and were very similar to that of calcined 3D samples. The XRD patterns of these two samples (not shown here) had no significant changes before and after exposure to air and were the typical 3D MWW patterns. Those results implied that the MWW zeolitic frameworks finally evolved from the layered precursor when the samples was outgassed at 200 °C, although a majority of structurally ordered PI molecules was still occluded in the zeolite at this time, as suggested by thermogravimetric analysis (TGA) in Table 5. Certainly, other samples outgassed at lower temperatures

with intermediate c values between that of precursor and the 3D structure should be an intermediate situation between the layered precursor and the condensed 3D structure. Similar inference was also drawn by Luca and co-workers using a combined XRD and computational study [46]. This meant that part of organic molecules were eliminated from the interlayer channels to cause the decrease in the interlayer distance upon vacuum-heating, and simultaneously Si-O-Si bands were partially formed between the layers.

Based on Table 5 and Fig. 4(B) we deduced that upon vacuum-heating the interlayer distance of the water washed precursor should reduce more rapidly than the condensation of the interlayer hydroxyl groups which was closely associated with vacuum-heating temperature, and the interlayer space was easy to reversibly expand when the samples were exposed to air atmosphere again. Inversely, the interlayer spacing decrease of EAOH-washed precursor was much slower and could synchronize with interlayer hydroxyl condensation upon vacuum-heating, which would make for the complete condensation of the interlayer silanols over the following calcination.

Fig. 5(A) compared the TGA results of Ti-MWW(P)-H₂O-100, Ti-MWW(P)-EAOH-100 and the corresponding acid-treated samples. The weight loss of Ti-MWW(P)-H₂O-100 was slightly smaller than that of Ti-MWW(P)-EAOH-100. The exothermic peak, usually believed to be attributed to the removal of PI molecules sited at the interlayer space, was around 380 °C for Ti-MWW(P)-H₂O-100 and about 405 °C for Ti-MWW(P)-EAOH-100. The exothermic peak at lower temperature suggested that the combustion of organic molecules in interlayer space of Ti-MWW(P)-H₂O-100 should be easier than Ti-MWW(P)-EAOH-100. This result matched well with the conclusion drawn from the analysis of the vacuum-heated samples above.

The weight loss of the corresponding acid-treated samples greatly reduced compared with the corresponding precursors. It meant that a large part of SDA molecules were removed by acid-treatment from both the water washed precursor and the EAOH washed precursor. Moreover, the TG curves showed that the weight loss of water washed samples was much greater than that of EAOH washed samples. This implied that the amount of PI molecules occluded in the former was much larger than in the latter. This part of PI molecules which was difficult to be removed by acid washing

Table 5

Weight loss of the vacuumed-heated samples.

Vacuum temperature (°C)	Weight loss in 200–700 °C (w%)		Weight loss in 200–400 °C (w%)		Weight loss by vacuum-heating in 200–400 °C (w%)	
	EAOH ^a	H ₂ O ^b	EAOH ^a	H ₂ O ^b	EAOH ^a	H ₂ O ^b
					— ^c	— ^c
— ^c	14.5	14.1	9.9	9.2	0	0
110	14.5	13.8	9.6	8.4	3.3	8.8
125	14.1	12.8	9.1	7.6	8.5	17.2
150	13.3	11.7	8.0	6.8	19.5	26.5
200	12.0	10.8	7.1	5.8	28.2	37.7

^a Sample prepared from Ti-MWW(P)-EAOH-100.^b Sample prepared from Ti-MWW(P)-H₂O-100.^c Precursor dried at 100 °C.

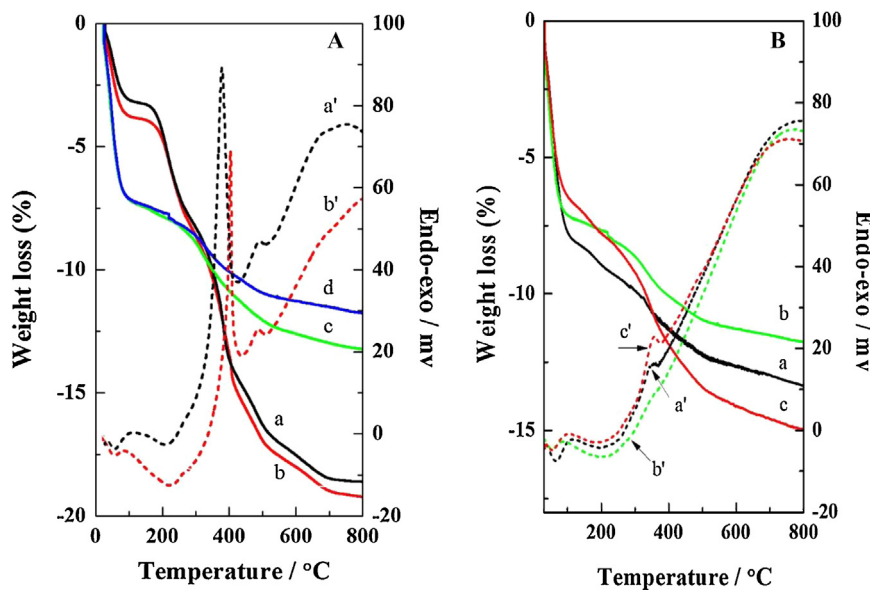


Fig. 5. (A) TG/DTA profiles of precursors Ti-MWW (P)-H₂O-100 (a, a') and Ti-MWW (P)-EOH-100 (b, b') and corresponding acid-treated samples Ti-MWW(A)-H₂O-100 (c), Ti-MWW(A)-EOH-100 (d); (B) TG/DTA profiles of the acid-treated samples prepared from EOH-washed precursors dried at 50 °C (a and a'), 100 °C (b and b') and 150 °C (c and c').

and tightly occluded in interlayer void space of the water washed sample would inevitably interrupt the further condensation of the interlayer hydroxyl groups upon the following calcination.

Fig. 4(B) compared the TGA results of the acid-treated samples prepared from the Ti-MWW(P)-OH dried at 50, 100 and 150 °C. The total weight loss of these three acid-treated samples was Ti-MWW(A)-OH-100 < Ti-MWW(A)-OH-50 < Ti-MWW(A)-OH-150, although the weight loss in the corresponding precursors was Ti-MWW(P)-OH-50 > Ti-MWW(P)-OH-100 > Ti-MWW(P)-OH-150 (not shown here) as expected. This result meant that the drying temperature would affect the PI amount occluded in the acid-treated samples and the lowest amount of PI was kept in the 100 °C dried sample. It was most noteworthy that very obvious peaks in the range of 300–400 °C were observed in the DTA curves of Ti-MWW(A)-OH-50 and Ti-MWW(A)-OH-150 but disappeared in the curve of Ti-MWW(A)-OH-100. This implied that after acid-treatment very few PI molecules were occluded in the interlayer void space of Ti-MWW(A)-OH-100, which certainly made for the completely condensation of interlayer hydroxyl groups and the formation of the perfect 3D structure.

5. Conclusion

Ti-MWW, originated from the corresponding flexible lamellar precursor, was always less hydrophobic because of the incomplete interlayer dehydroxylation. This study showed a very easy and efficient method to enhance the hydrophobicity and improve the catalytic activity of Ti-MWW by controlling the preparation conditions. Using organic solution especially EAOH instead of water to wash the wet lamellar precursor would change the interaction between SDA and the network of Ti-MWW precursor, and would synchronize the interlayer hydroxyl condensation with the decrease of interlayer distance mainly caused by SDA leaching. After acid-treatment, less SDA was kept in the EAOH washed sample and 3D-MWW with less defects was formed by calcination. Both drying temperature and acid-treatment would also affect the amount of SDA occluded in the interlayer void space of the acid-treated samples and then further affect the final interlayer hydroxyl condensation upon the following calcination. The lower drying temperature is favorable to unequal interlayer dehydroxylation to

form MCM-56, while higher drying temperature such as 150 °C not only cause the formation of anatase phase in the calcined samples but also occluded more SDA molecules in the acid-treated samples which greatly affect the further interlayer hydroxyl condensation upon the calcination. Ti-MWW-OH-100 containing the lowest amount of silanols and less defect sites showed the highest catalytic activity in 1-hexene oxidation.

Appendix A. Supplementary data

Supplementary data associated with this article can be found, in the online version, at <http://dx.doi.org/10.1016/j.apcata.2015.07.003>

References

- [1] M. Taramasso, G. Perego, B. Notari, US Patent 4,410,501, to S.P.A. Snamprogetti (1983).
- [2] A.J.H.P. van der Pol, A.J. Verduyn, J.H.C. van Hooff, *Appl. Catal. A* 92 (1992) 113–130.
- [3] F. Maspero, U. Romano, *J. Catal.* 146 (1994) 476–482.
- [4] R.S. Reddy, J.S. Reddy, R. Kumar, P. Kumar, *J. Chem. Soc. Chem. Commun.* 2 (1992) 84–85.
- [5] M. Ogura, S.I. Nakata, E. Kikuchi, M. Matsukata, *J. Catal.* 199 (2001) 41–47.
- [6] B. Notari, *Adv. Catal.* 41 (1996) 253–334.
- [7] J.S. Reddy, R. Kumar, *J. Catal.* 130 (1991) 440–446.
- [8] P. Wu, T. Tatsumi, T. Komatsu, T. Yashima, *J. Catal.* 202 (2001) 245–255.
- [9] P. Wu, T. Komatsu, T. Yashima, *J. Phys. Chem.* 100 (1996) 10316–10318.
- [10] H. Xu, Y.T. Zhang, H.H. Wu, X.M. Liu, X.H. Li, J.G. Jiang, M.Y. He, P. Wu, *J. Catal.* 281 (2011) 263–272.
- [11] F. Jin, S.Y. Chen, L.Y. Jang, J.F. Lee, S. Cheng, *J. Catal.* 319 (2014) 247–257.
- [12] M.A. Camblor, A. Corma, J. Pérez-Pariente, *Zeolites* 13 (1993) 82–87.
- [13] A. Corma, M.A. Camblor, P. Esteve, A. Martínez, J. Pérez-Pariente, *J. Catal.* 145 (1994) 151–158.
- [14] T. Blasco, M.A. Camblor, A. Corma, J. Pérez-Pariente, *J. Am. Chem. Soc.* 115 (1993) 11806–11813.
- [15] B. Dartt, C.B. Khouw, H.-X. Li, M.E. Davis, *Microporous Mater.* 2 (1994) 425–437.
- [16] T. Blasco, A. Corma, M.T. Navarro, J.P. Pariente, *J. Catal.* 156 (1995) 65–74.
- [17] A. Corma, M. Iglesias, F. Sánchez, *Catal. Lett.* 39 (1996) 153–156.
- [18] A. Corma, M.T. Navarro, J. Pérez Pariente, *J. Chem. Soc. Chem. Commun.* (1994) 147–148.
- [19] M.L. Pena, V. Dellarocca, F. Rey, A. Corma, S. Coluccia, L. Marchese, *Microporous Mesoporous Mater.* 44 (2001) 345–356.
- [20] A. Bhaumik, T. Tatsumi, *J. Catal.* 189 (2000) 31–39.
- [21] L. Zhang, H.C.L. Abbenhuysen, G. Gerritsen, N. Ni Bhriain, P. Magusin, B. Mezari, W. Han, R.A. van Santen, Q.H. Yang, C. Li, *Chem. Eur. J.* 13 (2007) 1210–1221.
- [22] F. Berube, B. Nohair, F. Kleitz, S. Kaliaguine, *Chem. Mater.* 22 (2010) 1988–2000.

- [23] P. Wu, T. Tatsumi, T. Komatsu, T. Yashima, *Chem. Mater.* 14 (2002) 1657–1664.
- [24] F. Carniato, E. Boccaleri, L. Marchese, *Dalton Trans.* 1 (2008) 36–39.
- [25] C.C. Huang, Z.J. Wei, L. Zhang, X. Luo, H.B. Ren, M.M. Luo, *J. Porous Mater.* 20 (2013) 1017–1022.
- [26] C.B. Khouw, C.B. Dartt, J.A. Labinger, M.E. Davis, *J. Catal.* 149 (1994) 195–205.
- [27] S. Park, K.M. Cho, M.H. Youn, J.G. Seo, J.C. Jung, S.H. Baek, T.J. Kim, Y.M. Chung, S.H. Oh, I.K. Song, *Catal. Commun.* 9 (2008) 2485–2488.
- [28] A. Corma, P. Esteve, A. Martinez, *J. Catal.* 161 (1996) 11–19.
- [29] C.H. Xu, T.H. Jin, S.H. Jhung, J.S. Hwang, S.E. Park, *Catal. Today* 111 (2006) 366–372.
- [30] T. Blasco, M.A. Cambor, A. Corma, P. Esteve, J.M. Guil, A. Martinez, J.A. Perdigon-Melon, S. Valencia, *J. Phys. Chem. B* 102 (1998) 75–88.
- [31] T. Tatsumi, K.A. Koyano, N. Igarashi, *Chem. Commun.* (1998) 325.
- [32] K. Yasutaka, A. Junya, M. Keisuke, E. Taro, K. Takashi, M. Kohsuke, Y. Hiromi, *J. Catal.* 285 (2012) 223–234.
- [33] K. Nakatsuka, K. Mori, S. Okada, S. Ikurumi, T. Kamegawa, H. Yamashita, *Chem. Eur. J.* 20 (2014) 8348–8354.
- [34] A. Wróblewska, A. Fajdek, E. Milchert, B. Grzmil, *Pol. J. Chem. Technol.* 12 (2010) 29–34.
- [35] A. Wróblewska, A. Fajdek, *J. Adv. Oxid. Technol.* 14 (2011) 122–130.
- [36] A. Wróblewska, G. Wójtowicz, E. Makuch, *J. Adv. Oxid. Technol.* 14 (2011) 267–275.
- [37] A. Fajdek, A. Wróblewska, E. Milchert, *Int. J. Chem. React. Eng.* 10 (2012) 1–16.
- [38] S. Maheshwari, E. Jordan, S. Kumar, F.S. Bates, R.L. Penn, D.F. Shantz, M. Tsapatsis, *J. Am. Chem. Soc.* 130 (2008) 1507–1516.
- [39] A. Corma, U. Diaz, V. Fornes, J.M. Guil, J. Martinez-Triguero, E.J. Creyghton, *J. Catal.* 191 (2000) 218–224.
- [40] A. Corma, V. Fornes, S.B. Pergher, T.L.M. Maesen, J.G. Buglass, *Nature* 396 (1998) 353–356.
- [41] S. Inagaki, H. Imai, S. Tsujiuchi, H. Yakushiji, T. Yokoi, T. Tatsumi, *Microporous Mesoporous Mater.* 142 (2011) 354–362.
- [42] L.L. Wang, Y.M. Liu, W. Xie, H.H. Wu, X.H. Li, M.Y. He, P. Wu, *J. Phys. Chem. C* 112 (2008) 6132–6138.
- [43] Y. Wang, Y.M. Liu, L.L. Wang, H.H. Wu, X.H. Li, M.Y. He, P. Wu, *J. Phys. Chem. C* 113 (2009) 18753–18760.
- [44] H.M. Rietveld, *J. Appl. Crystallogr.* 2 (1969) 65–71.
- [45] M.E. Leonowicz, J.A. Lawton, S.L. Lawton, M.K. Rubin, *Science* 264 (1994) 1910.
- [46] L. Palin, G. Croce, D. Viterbo, M. Milanesio, *Chem. Mater.* 23 (2011) 4900–4909.